Journal of Materials Chemistry C

ROYAL SOCIETY OF CHEMISTRY

PAPER

View Article Online
View Journal | View Issue

Cite this: J. Mater. Chem. C, 2023, 11, 16368

Systematic investigation *via* controlling the energy gap of the local and charge-transfer triplet state for enabling high efficiency thermally activated delayed fluorescence emitters†

Nisha Yadav, Upasana Deori, Ezhakudiyan Ravindran, Bahadur Sk and Pachaiyappan Rajamalli *

Thermally activated delayed fluorescence (TADF) emitters have evolved as a certified candidate in light generation technologies for producing efficient organic light-emitting diodes (OLEDs) on account of their 100% internal quantum efficiency (IQE) *via* reverse intersystem crossing (RISC) and toxic metal-free design. The fast rate of RISC (k_{RISC}) is the ultimate requirement of an efficient TADF emitter, which can be achieved by minimizing the singlet–triplet energy gap (ΔE_{ST}). Here, four donor–acceptor type TADF emitters namely **3BPy-*m*DCz**, **3BPy-*m*DTA**, **3BPy-*m*DMAC**, and **3BPy-*m*DPT** were synthesized based on benzoyl pyridine (3BPy) as an unaltered acceptor and varying the donor strength ranging from carbazole to phenothiazine. These emitters show low ΔE_{ST} values forecasting their TADF nature. The ΔE_{ST} values decreased from 0.22 to 0.14 eV upon increasing the donor strength. The maximum external quantum efficiency (EQE) of 18.7% for **3BPy-*m*DCz**, 22.5% for **3BPy-*m*DTA**, 13.8% for **3BPy-*m*DMAC** and 2.1% for **3BPy-*m*DPT** was obtained. These drastic differences in the performances of **3BPy-*m*DTA** and **3BPy-*m*DPT** are due to the locally excited ^{3}LE(T_2) intermediate state between the lowest singlet (S_1) and triplet (T_1). Among **3BPy-*m*DMAC** and **3BPy-*m*DPT**, the efficiency of **3BPy-*m*DMAC** is superior due to less CT character and high photoluminescence quantum yield (PLQY). This work paves a new direction for efficient TADF molecular design by indicating the role of the intermediate triplet state (^{3}LE) despite possessing high ΔE_{ST} values.

Received 14th October 2023,
Accepted 6th November 2023

DOI: 10.1039/d3tc03752e

rsc.li/materials-c

1. Introduction

Light-emitting materials with thermally activated delayed fluorescence (TADF) have attracted a great deal of interest owing to the utilization of their potential features in next-generation organic light-emitting diodes (OLEDs).[1,2] TADF emitters have emerged as a promising technology and prospective alternative to phosphorescent emitters for OLEDs due to their ability to reach 100% internal quantum efficiency (IQE) without the use of rare-earth metals.[3–8] Efficient up-conversion *via* reverse intersystem crossing (RISC) is needed in TADF emitters to achieve a reduction in triplet–triplet annihilation (TTA), which is the primary cause of degradation in phosphorescent emitters.[9,10] Hence, fast RISC is required to acquire high-performance TADF OLEDs over phosphorescent OLEDs. Therefore, a small energy gap between the lowest singlet (S_1) and triplet (T_1) excited states ($\Delta E_{ST} < 0.2$ eV) is required to facilitate efficient exciton up-conversion from $T_1 \rightarrow S_1$ *via* reverse intersystem crossing.[11,12] A commonly used TADF molecular design strategy is constructing a twisted molecular conformation with various donor and acceptor units in order to separate the highest occupied molecular orbital (HOMO) and lowest unoccupied molecular orbital (LUMO) and achieve small ΔE_{ST}.[13–15] Furthermore, increasing the steric hindrance and highly twisted conformation and breaking conjugation in the molecular geometry are also the most effective pathways to fulfill the above criterion *via* minimizing electron exchange energy splitting S_1 from T_1.[16–19]

According to the Franck–Condon transition principle and Fermi's golden rule, high oscillator strength is needed for high photoluminescence quantum yield (Φ_{PL}), which can be achieved by a large overlap degree of the frontier molecular orbital.[2,18,20] Upon increasing the donor strength we can get low ΔE_{ST} but it suffers from low Φ_{PL} due to which efficient TADF can't be obtained. The main reason behind this is the weak spin–orbit coupling (SOC) between S_1 and T_1 due to the charge transfer (CT) character of states leading to inefficient RISC.[21–23] Hence, low

Materials Research Centre, Indian Institute of Science Bangalore, C. V. Raman Road, Bengaluru, Karnataka, 560012, India. E-mail: rajamalli@iisc.ac.in

† Electronic supplementary information (ESI) available. See DOI: https://doi.org/10.1039/d3tc03752e

ΔE_{ST} is not the sole criteria to achieve efficient TADF emitters. There are several requirements for efficient TADF materials but the core parameter is still the fast rate of RISC (k_{RISC}) as well as radiative de-activation (k_r). For efficient TADF, both small ΔE_{ST} and considerable k_{RISC} have to be realized simultaneously.

SOC in purely organic emitters has drawn considerable attention due to its tendency to facilitate RISC. According to the El-Sayed rule, SOC increases with the difference in nature of the excited states (charge transfer excited state, CT *vs*. localized excited state, LE).[24] In most of the cases, S_1 displays predominantly CT character (^{1}CT) and therefore the vicinity of the localized triplet state (^{3}LE) will increase SOC.[25,26] RISC proceeds *via* vibronic coupling between $^3CT(T_1)$ and $^3LE(T_2)$ states followed by SOC between $^1CT(S_1)$ and $^3LE(T_2)$.[23,27,28] Although there are a range of theoretical reports explaining the role of intermediate states in enhancing SOC, it is less explored experimentally in purely organic emitters without any heavy atom. To overcome this bottleneck, the optimum molecular design for efficient TADF emitters should be well understood and proper guidelines for rational molecular design are highly desired for the practical application of TADF-based OLEDs.

In this study, we designed and synthesized four donor–acceptor based TADF molecules **3BPy-*m*DCz**, **3BPy-*m*DTA**, **3BPy-*m*DMAC** and **3BPy-*m*DPT** (Scheme 1). Benzoyl pyridine (3BPy) acts as an unaltered acceptor moiety while the donor moiety varies from carbazole to phenothiazine. The ΔE_{ST} values also decreased from 0.22 to 0.14 eV, and hence improved performance was expected. By adopting the above emitters as dopants, we acquire blue to yellow TADF OLEDs. However, the maximum EQEs of 18.7% for **3BPy-*m*DCz**, 22.5% for **3BPy-*m*DTA**, 13.8% for **3BPy-*m*DMAC** and 2.1% for **3BPy-*m*DPT** were obtained. **3BPy-*m*DCz** and **3BPy-*m*DTA** possess an intermediate $^3LE(T_2)$ state between S_1 and T_1 which facilitates both k_{RISC} and k_r and hence these emitters show high efficiency as compared to other emitters. High performance can be achieved in spite of having a relatively large ΔE_{ST} value *via* systematically optimising the number and nature of intermediate states between S_1 and T_1. This work highlights that increasing the donor strength or reducing the ΔE_{ST} is not the only desired criteria to get efficient TADF while the position/nature of the additional triplet state (^{3}LE/^{3}CT) state is equally important in enhancing the efficiency of TADF emitters.[29,30]

2. Results and discussion

2.1. Theoretical calculation

To understand the effect of variation of the donor moieties, density functional theory (DFT) and time-dependent DFT (TD-DFT) calculations were performed using the B3LYP/6-31G(d,p) method. The atomic delocalization of the S_0 geometry and excited-state energy levels of the four designed molecules was then conducted. Fig. 1 shows the optimized molecular structure along with the molecular orbital distribution of the HOMO and the LUMO of these molecules. The LUMOs were mainly residing on the acceptor unit (3BPy) due to its electron withdrawing nature while the HOMOs were widely localized on the donor groups and extended to the phenyl ring based on their descending order of donor strengths, which are crucial for the occurrence of delayed fluorescence. The calculated excitation energies and HOMO/LUMO energy levels of the S_1 and T_1 excited states are shown in Table S1, ESI.† The FMO distributions resulted in reduced ΔE_{ST} values as 0.19, 0.24, 0.03 and 0.02 eV for **3BPy-*m*DCz**, **3BPy-*m*DTA**, **3BPy-*m*DMAC** and **3BPy-*m*DPT**, respectively. The small ΔE_{ST} values suggest that molecules can exhibit TADF properties. Overlap between the HOMO and LUMO retains high oscillator strength (f) in

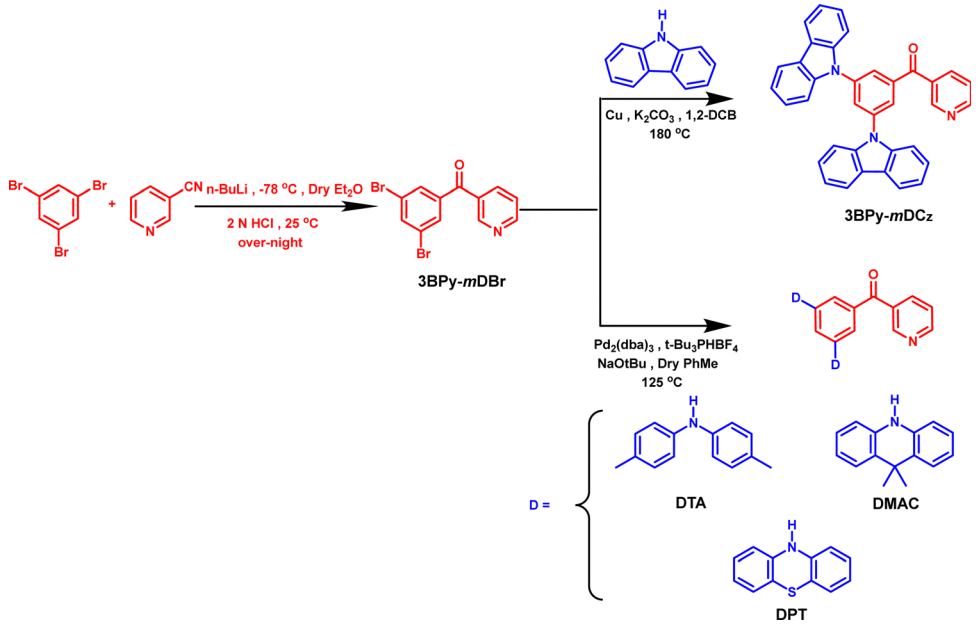

Scheme 1 Synthesis of **3BPy-*m*DCz**, **3BPy-*m*DTA**, **3BPy-*m*DMAC** and **3BPy-*m*DPT**.

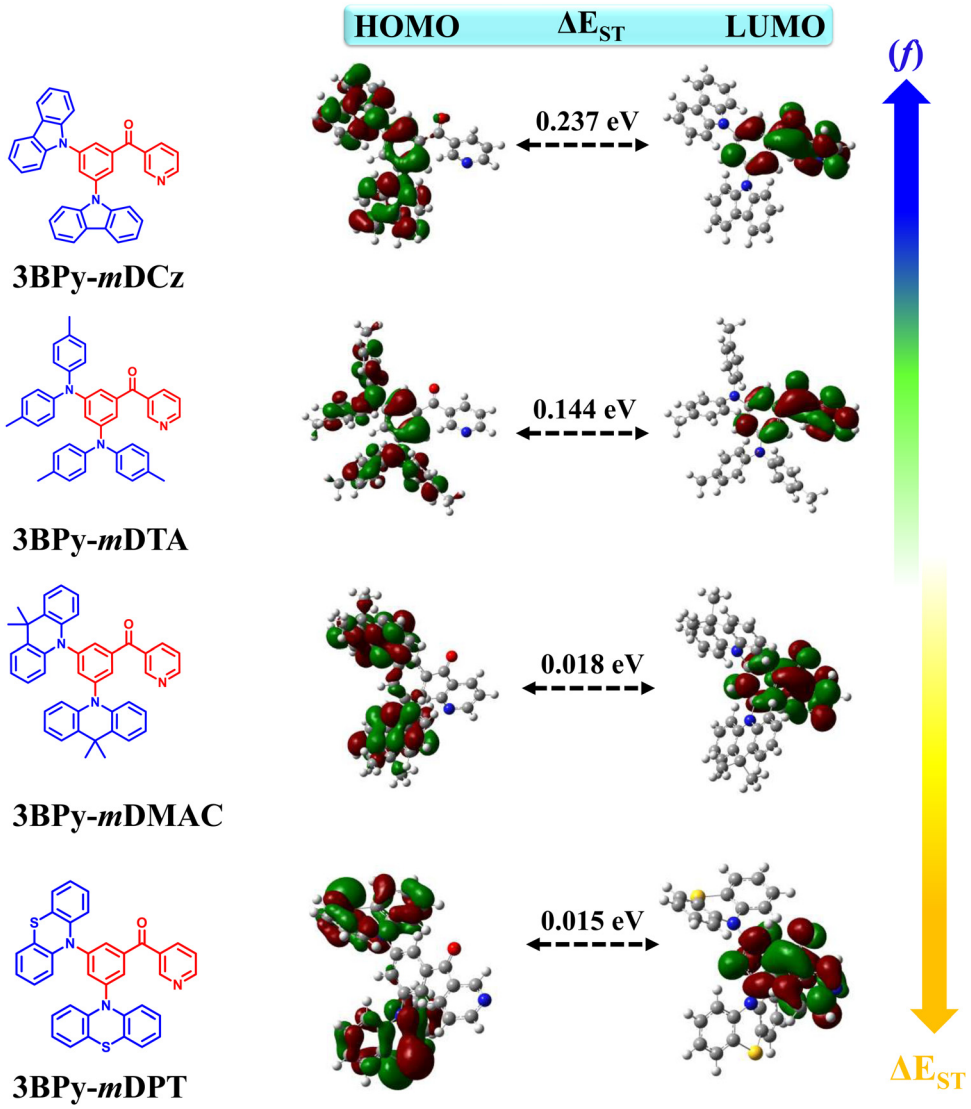

Fig. 1 The distribution of the molecular orbital of the HOMO and LUMO with a calculated S_1 and T_1 energy gap (ΔE_{ST}). The right side top and bottom of the arrow marks indicate the enhancement of oscillator strengths (f) and reduction of ΔE_{ST} when increasing the donor strength.

3BPy-*m*DCz and **3BPy-*m*DTA** as compared to other derivatives, which is helpful to maintain a high radiative decay rate (k_r).[31]

2.2. Synthesis and characterization

The designed compounds were synthesized in high yields *via* the Ullmann coupling reaction and Buchwald–Hartwig amination of (3-bromobenzoyl)pyridine with various donor moieties. The synthetic routes are displayed in Scheme 1 while the detailed synthetic procedures and characterization data are given in the ESI.† All the compounds were further purified by temperature-gradient vacuum sublimation and chemical structures are confirmed by ^{1}H, ^{13}C NMR and high-resolution mass spectrometry (HRMS) (Fig. S9–S18, ESI†).

2.3. Thermal and electrochemical properties

All four materials (**3BPy-*m*DCz**, **3BPy-*m*DTA**, **3BPy-*m*DMAC** and **3BPy-*m*DPT**) show good thermal stability with decomposition temperatures (T_d) corresponding to 5 wt% loss in the range of 331–422 °C (Fig. S1, ESI† and Table 1). The glass transition was not obtained during differential scanning calorimetry (DSC) analysis. These high stabilities are important for stable film formation.

The energy band gap (E_g) that is being calculated from the absorption onset for all emitters is listed in Table S2, ESI.† The electrochemical properties of all the four emitters were examined by cyclic voltammetry (CV) as shown in Fig. S2, ESI.†[32] All emitters exhibited two reversible oxidation waves confirming the oxidation of both the donor moieties. The HOMO energy level came out to be −5.26, −5.14, −4.95 and −5.03 eV for **3BPy-*m*DCz**, **3BPy-*m*DTA**, **3BPy-*m*DMAC** and **3BPy-*m*DPT**, respectively, as listed in Table S2, ESI.† Upon increasing the donor strength, the HOMO level increases due to the increase in the electron donating ability and this trend matches with theoretical values. The calculated LUMO energy

Table 1 Photophysical properties of **3BPy-*m*DCz**, **3BPy-*m*DTA**, **3BPy-*m*DMAC** and **3BPy-*m*DPT**

Compound	λ_{abs}[a] (nm)	λ_{PL}[b] (nm) (sol/film)	λ_{Ph}[c] (nm) (sol/film)	ΔE_{ST}[d] (eV) (sol/film)	ϕ_{PL}[e] (air/vac)	τ_P[f] (ns)	τ_D[g] (μs) (air/vac)	T_d[h] (°C)
3BPy-*m*DCz	338, 372	456/463	472/493	0.13/0.22	56/59	10.3	118.8/340.3	381
3BPy-*m*DTA	300, 424	522/532	551/576	0.18/0.20	16/48	6.8	119.7/785.7	350
3BPy-*m*DMAC	287, 401	534/528	547/535	0.15/0.11	34/53	30.9	6.6/9.2	331
3BPy-*m*DPT	319, 425	—/551	—/565	—/0.14	7/12	16.1	13.8/41.4	422

[a] Absorbance peaks. [b] Steady state emission maxima at room temperature. [c] Phosphorescence emission maxima in solution measured in toluene (Tol) (1×10^{-5} M) and doped film (7 wt% of emitter:host) at 77 K. [d] Singlet–triplet energy gap. [e] Absolute PLQY in doped films using an integrating sphere under air and vacuum atmosphere. [f] Prompt lifetime. [g] Delayed lifetime at room temperature under air and vacuum. [h] Thermal decomposition temperature under a N_2 atmosphere.

levels were −2.26, −2.54, −2.25 and −2.65 eV, respectively, by taking into account the HOMO and E_g values.

2.4. Photophysical properties

Photophysical properties of **3BPy-*m*DCz**, **3BPy-*m*DTA**, **3BPy-*m*DMAC** and **3BPy-*m*DPT** in 10 μM toluene solution are shown in Fig. 2 and Fig. S3, ESI.† All the compounds display similar absorption spectral profiles with a strong absorption band observed before 350 nm associated with the π–π and n–π* transitions[33] and relatively weak and structureless broadband absorption peaks observed at 372, 425, 394 and 423 nm for **3BPy-*m*DCz**, **3BPy-*m*DTA**, **3BPy-*m*DMAC** and **3BPy-*m*DPT**, respectively, which is associated with the intramolecular charge transfer (ICT) from the donor moieties to the acceptor moiety.[34] The PL spectra were measured in toluene (10 μM) at room temperature (RT) and **3BPy-*m*DCz**, **3BPy-*m*DTA** and **3BPy-*m*DMAC** show slightly broad and structureless emission. **3BPy-*m*DPT** is not emissive in the solution state, and hence the emission spectra couldn't be studied in the solution state. The summary of the photophysical properties is depicted in Table 1. It is noteworthy that the emission maximum peaks of **3BPy-*m*DCz**, **3BPy-*m*DTA** and **3BPy-*m*DMAC** have been observed at 456, 522 and 534 nm, respectively. Furthermore, the S_1 energies were calculated to be 3.08, 2.71 and 2.76 eV, respectively from the onset of the fluorescence spectra. The phosphorescence spectra of these systems were measured at 77 K in toluene (10 μM) with peaks centered at 472, 551 and 547 nm, respectively, as shown in Fig. 2. The phosphorescence spectra of these emitters showed broad structureless emission, which indicates that their phosphorescence emission originates from the CT triplet state of these molecules. Furthermore, the T_1 energies were calculated to be 2.95, 2.53 and 2.61 eV, respectively from the onset of their phosphorescence spectra. Therefore, the ΔE_{ST} was estimated in the range of 0.13, 0.18 and 0.15 eV, respectively, as shown in Table 1. The small ΔE_{ST} of these molecules suggests that these emitters may have TADF properties. The solvatochromic study was done by taking emission spectra in various solvent polarities as shown in Fig. S4, ESI.† Significantly, their PL spectra are concomitantly red-shifted and slightly broadened with the increase of the solvent polarity, which clearly indicates that these molecules are CT in nature and the S_1 state is stabilized upon increasing solvent polarity.

In order to get an overview of the optical properties in the thin film, a photophysical study was carried out in doped thin film. DPEPO (triplet energy of 3.0 eV) host was taken for

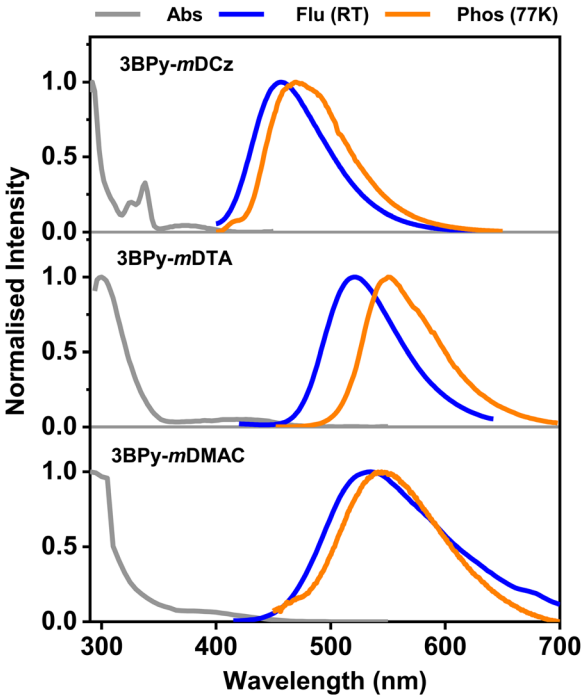

Fig. 2 UV-Vis absorption, fluorescence (RT), and phosphorescence (77 K) spectra of **3BPy-*m*DCz**, **3BPy-*m*DTA**, and **3BPy-*m*DMAC** respectively in toluene (Tol) (1×10^{-5} M).

3BPy-*m*DCz while *m*CBP (triplet energy of 2.8 eV) host was taken for the remaining three emitters, which confine triplet excitons and efficiently suppress backward energy transfer from the guest to the host materials. The doped films with 7 wt% doping concentration give blue to yellow emission with an emission peak of 463 nm for **3BPy-*m*DCz**, 532 nm for **3BPy-*m*DTA**, 528 nm for **3BPy-*m*DMAC** and 551 nm for **3BPy-*m*DPT**. The fluorescence and phosphorescence spectra of the co-doped films were measured and presented in Fig. 3 and Table 1. The ΔE_{ST} values measured from the onset of the PL spectra at RT and phosphorescence spectra at 77 K are 0.22, 0.20, 0.11 and 0.14 eV for **3BPy-*m*DCz**, **3BPy-*m*DTA**, **3BPy-*m*DMAC** and **3BPy-*m*DPT**, respectively. The ΔE_{ST} gradually decreased upon increasing the donor strength. These values are low enough to have efficient up-conversion of T_1 excitons to the S_1 state.[35]

Furthermore, the PLQY of the doped films was measured using an integrating sphere under the air and a N_2 atmosphere. Under air, the PLQYs of the doped films came out to be 56% for

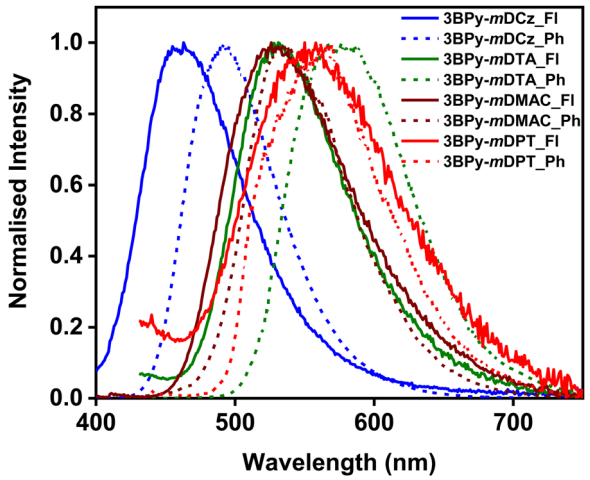

Fig. 3 Fluorescence (Fl) and phosphorescence (Ph) spectra of 7 wt% **3BPy-*m*DCz**:DPEPO, **3BPy-*m*DTA**:*m*CBP, **3BPy-*m*DMAC**:*m*CBP and **3BPy-*m*DPT**:*m*CBP doped film.

3BPy-*m*DCz, 16% for **3BPy-*m*DTA**, 34% for **3BPy-*m*DMAC** and 7% for **3BPy-*m*DPT** while under a N_2 atmosphere, the PLQY increased to 59% for **3BPy-*m*DCz**, 48% for **3BPy-*m*DTA**, 53% for **3BPy-*m*DMAC** and 12% for **3BPy-*m*DPT**. The PLQY enhancement in a N_2 atmosphere compared to air is likely due to the suppression of triplet exciton quenching by atmospheric oxygen.[36,37] The corresponding PLQY values decreased as the donor strength increased on account of the increase in CT character.[22] The decrease of PLQY in the presence of oxygen supports that these materials possess unambiguous TADF properties and suggests that the T_1 states of these molecules are readily quenched by the triplet ground state oxygen molecules. The quenching of T_1 by oxygen leads to the quenching of the delayed fluorescence and a decrease in the emission intensity.

To further reveal the effect of donor strength on the TADF properties of the emitters, we studied transient photoluminescence decay (TRPL) of the doped films (7 wt% **3BPy-*m*DCz**, **3BPy-*m*DTA**, **3BPy-*m*DMAC** and **3BPy-*m*DPT**) which were fabricated by vacuum deposition. As shown in Fig. 4, the transient decay curves show two components. The first one is the prompt fluorescence decay from S_1 to S_0 with a lifetime τ_P and the second one is delayed emission with a lifetime τ_d, which can be rationalized as the thermal up-conversion of T_1 to S_1 through RISC followed by fluorescence to the S_0. **3BPy-*m*DCz** and **3BPy-*m*DTA** possess a shorter excited state prompt lifetime as compared to other derivatives. Furthermore, to confirm the TADF characteristics of these emitters, the temperature-dependent TRPL decay was measured. As shown in Fig. S5, ESI,† a temperature sweep between 200 to 298 K under vacuum was carried out. The delayed component increases with an increase of temperature from 200 K to 298 K (RT), which has concomitantly disclosed that the efficient exciton up-conversion occurred from T_1 to S_1 *via* RISC.

2.5. Electroluminescence performance

Devices were fabricated to investigate the electroluminescence (EL) properties using an optimized structure of ITO/NPB (30 nm)/TAPC (20 nm)/host:emitter (7 wt%) (30 nm)/PPT (10 nm)/TmPyPb (60 nm)/LiF (1 nm)/Al (100 nm), where the emitters are **3BPy-*m*DCz**, **3BPy-*m*DTA**, **3BPy-*m*DMAC** and **3BPy-*m*DPT**. The device architecture along with the molecular structure of all the entities is shown in Fig. S6, ESI.† In these devices, *N*,*N*′-bis(1-naphthyl)-*N*,*N*′-diphenyl-1,1′-biphenyl-4,4′-diamine (NPB) acts as the hole injection material, 1,1-bis[4-[*N*,*N*′-di(*p*-tolyl)amino]phenyl] cyclohexane (TAPC) acts as the hole transporting material as well as an exciton blocker and 1,3,5-tri(*m*-pyrid-3-yl-phenyl)benzene (TmPyPb) is the electron-transporting material.[38] Additionally, 2,8-bis(diphenyl-phosphoryl)-dibenzo[*b*,*d*]thiophene (PPT) has been used as an electron transport as well as hole blocking layer. Bis[2-(diphenylphosphino)phenyl]ether oxide (DPEPO) was taken as the host for **3BPy-*m*DCz**, 3,3′-bis(9*H*-carbazol-9-yl)-1,1′-biphenyl (*m*CBP) for **3BPy-*m*DTA** and 4,4′-bis(9*H*-carbazol-9-yl)-1,1′-biphenyl (CBP) for the remaining two emitters. Finally, lithium fluoride (LiF) was used as an electron injection layer and aluminium (Al) as the cathode. The EL characteristics of these four material-based OLED devices are displayed in Fig. 5 and the data are summarized in Table 2.

Fig. 5(a) shows normalised EL spectra of the four optimized OLEDs. On gradually enhancing the electron-donating capabilities,

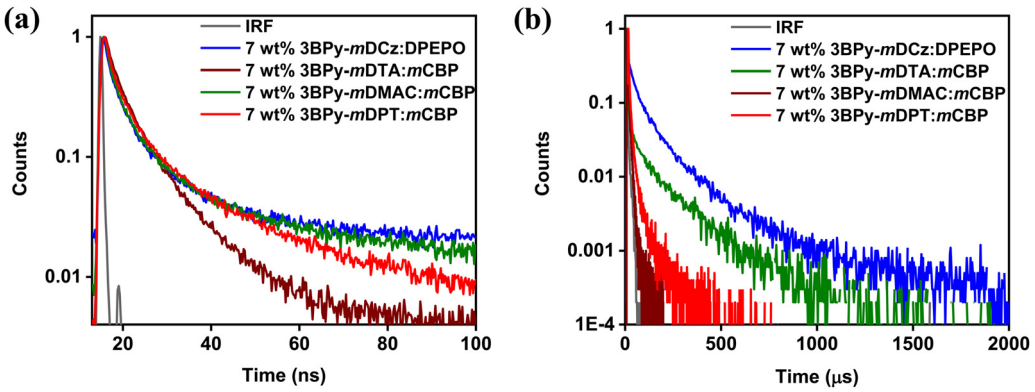

Fig. 4 Transient PL decays of DPEPO and *m*CBP host films doped with 7 wt% of emitter (a) prompt and (b) delayed component at 298 K.

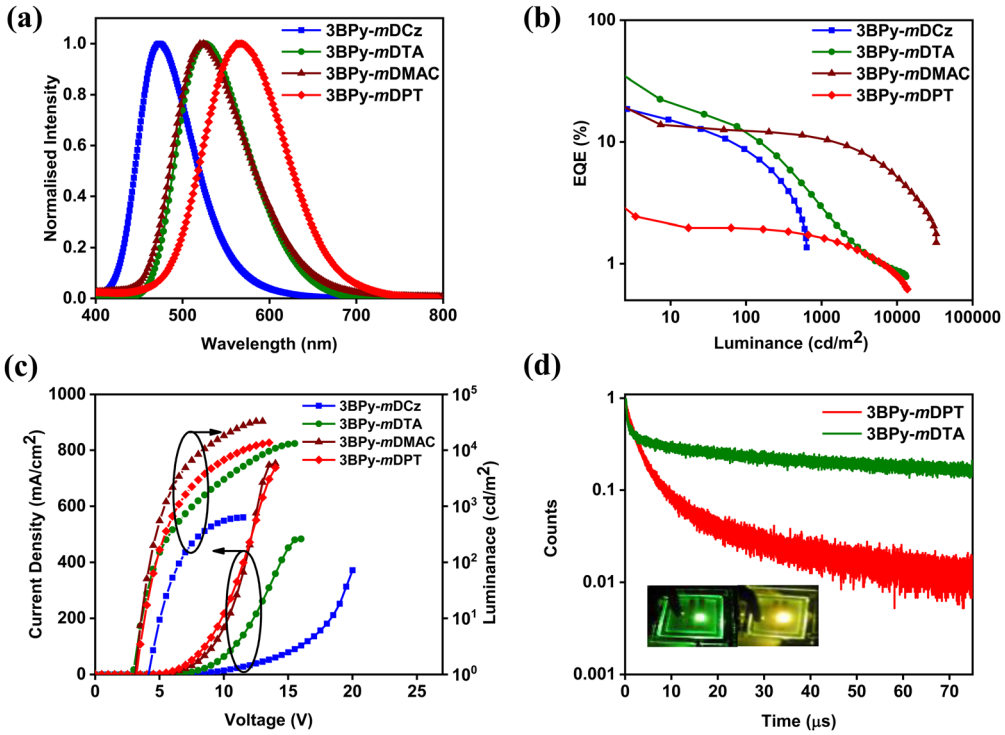

Fig. 5 (a) EL spectra; (b) EQE *versus* luminance characteristics (c) luminance–voltage–current density characteristics. (d) Transient EL spectra; inset is an EL illumination image of **3BPy-*m*DTA** (green emission) and **3BPy-*m*DPT** (yellow emission).

the emission peaks drastically shifted from blue emission for **3BPy-*m*DCz** with an EL λ_{max} of 473 nm, to green emission for **3BPy-*m*DTA** with an EL λ_{max} of 525 nm, green emission for **3BPy-*m*DMAC** with an EL λ_{max} of 523 nm and yellow emission for **3BPy-*m*DPT** with an EL λ_{max} of 566 nm showing resemblance to the PL spectra, as shown in Fig. S7, ESI.† As the donor strength is increased, charge transfer nature increases subsequently increasing the full width at half maximum (FWHM) value (as evident from the DFT also). The **3BPy-*m*DTA** based device shows higher FWHM value as compared to **3BPy-*m*DMAC** due to the flexibility of the DTA donor (Table 2). However, the EQE *vs.* luminance plot indicates that on increasing the donor strength, EQE decreases from 18.7% to 2.1% except for **3BPy-*m*DTA** which interestingly shows the highest EQE of 22.5% despite possessing larger ΔE_{ST}, as shown in Fig. 5(b). However, **3BPy-*m*DTA** possesses relatively higher efficiency roll-off as compared to other emitters on account of higher k_{ISC}, and hence longer excited lifetime leading to various exciton annihilation processes at high operating voltage. To confirm their TADF properties in the device under electrical excitation, the transient EL decay was measured for devices at RT, as shown in Fig. 5(d). The EL delayed component lasts for several tens of μs and this result strongly supports the existence of the TADF under electrical excitation.

In order to get deeper insights into the relative performance of all the emitters, Natural Transition Orbital (NTO) calculations for hole and electron distributions were obtained using the Multiwfn program package, as shown in Fig. S8, ESI.† In the case of **3BPy-*m*DCz** and **3BPy-*m*DTA**, there is the presence of an additional intermediate state (^{3}LE) between S_1 and T_1 while in the case of **3BPy-*m*DMAC** and **3BPy-*m*DPT** there is no additional intermediate state, as shown in Fig. 6. It is interesting to notice that the S_1 state of each emitter is predominantly CT in nature but in the case of **3BPy-*m*DTA**, it shows CT as well as LE nature. According to the NTO calculation, the nature of S_1 and T_1 excited states along with h/e overlap of **3BPy-*m*DTA** has a large distribution on the phenyl bridge as compared to other

Table 2 Electroluminescence properties of **3BPy-*m*DCz**, **3BPy-*m*DTA**, **3BPy-*m*DMAC** and **3BPy-*m*DPT**

Device[a]	λ_{EL}[b] (nm)	FWHM[c] (nm)	V_{on}[d] (V)	L_{max}[e] (cd m^{-2})	PE[f] (lm W^{-1})	CE[g] (cd A^{-1})	EQE[h] (%) (max/100/500)	CIE[i] (x, y)
3BPy-*m*DCz	473	68	4.0	635	21.9	31.5	18.7/8.4/2.8	(0.15, 0.21)
3BPy-*m*DTA	525	91	2.8	13 139	70.4	78.7	22.5/11.9/4.8	(0.29, 0.58)
3BPy-*m*DMAC	523	88	3.0	33 066	40.0	44.7	13.8/12.3/11.3	(0.31, 0.54)
3BPy-*m*DPT	566	102	3.3	13 685	6.0	6.8	2.1/1.9/1.8	(0.44, 0.51)

[a] Device configuration: ITO/NPB (30 nm)/TAPC (20 nm)/Emitter: host (7 wt%) (30 nm)/PPT (10 nm)/TmPyPb (60 nm)/LiF (1 nm)/Al (100 nm) where DPEPO was taken as the host for **3BPy-*m*DCz**, *m*CBP for **3BPy-*m*DTA**, and CBP for the remaining two emitters. [b] Electroluminescence maxima. [c] Full width at half maxima value. [d] Operating voltage at a brightness of 1 cd m^{-2}. [e] Maximum luminance. [f] Maximum power efficiency. [g] Maximum current efficiency. [h] External quantum efficiency at Max/100/500 cd m^{-2}. [i] Color coordinates (CIE 1931).

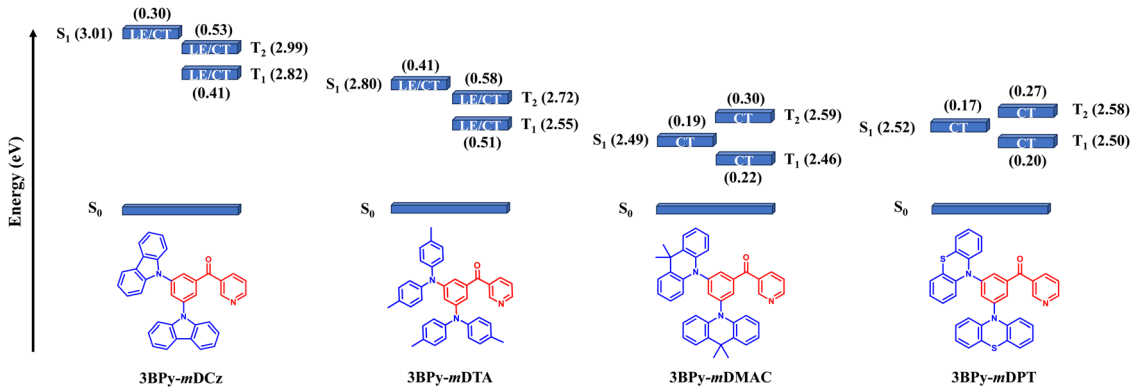

Fig. 6 Energy level diagram of excited states (S_1, T_1 and T_2) for **3BPy-*m*DCz**, **3BPy-*m*DTA**, **3BPy-*m*DMAC** and **3BPy-*m*DPT** where the value in brackets indicates the hole–electron overlap for the specified level.

emitters, as shown in Fig. 7. Therefore, it possesses the S_1 excited state with hybrid characteristics of local and charge-transfer excitations (CT/LE) for this particular molecular engineering.[39]

According to El-Sayed's rule, spin–orbit coupling (SOC) is forbidden between the same nature of states while it is allowed when the states have different nature.[29] **3BPy-*m*DCz** possesses a h–e overlap of ~0.53 (more LE character) and ~0.41 (less LE character), respectively, for the T_2 and T_1 states enabling more mixing between these states. On the other hand, **3BPy-*m*DTA** possesses a h–e overlap of ~0.58 (more LE character) and ~0.51 (more LE character) for the T_2 and T_1 state enabling less mixing. Since the S_1 state of **3BPy-*m*DTA** has more LE nature (~0.41) as compared to **3BPy-*m*DCz** (0.30), a higher prompt efficiency is expected for **3BPy-*m*DTA**. Similarly, the h–e overlap for **3BPy-*m*DMAC** and **3BPy-*m*DPT** is ~0.22 and ~0.20, respectively for the T_1 state. Due to less CT character of T_1 in **3BPy-*m*DMAC** as compared to **3BPy-*m*DPT**, higher efficiency is expected for **3BPy-*m*DMAC**. The combination of the above factors feasibly allows the **3BPy-*m*DTA** to maintain the highest *f* values and exhibit maximum efficiency irrespective of the large ΔE_{ST} value. These findings highlight that randomly choosing a combination of D and A moieties will not be beneficial but the nature and number of intermediate states should also be considered in enhancing up-conversion and hence efficiency.

In order to validate this experimentally, the main kinetic parameters including the rate constants of fluorescence radiative decay (k_r), non-radiative internal conversion (k_{IC}), ISC (k_{ISC}) and RISC (k_{RISC}) are calculated according to eqn (S1)–(S5), ESI† which is summarised in Table 3. A higher value of k_r and k_{RISC} is needed to achieve high performance. **3BPy-mDCz** shows the highest value of k_r but k_{RISC} is relatively slow. Similarly, for **3BPy-*m*DMAC** k_{RISC} is the highest but k_r is small. In addition, the presence of the T_2 state in between T_1 and S_1 helps to get the optimum value of k_{RISC} and simultaneously higher h–e overlap leads to higher prompt efficiencies for TADF emitters.[40]

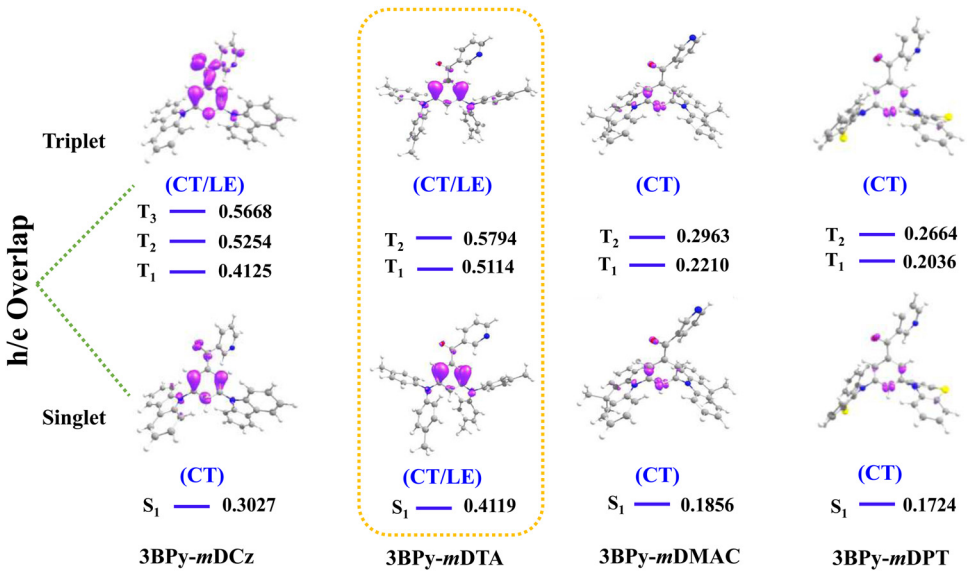

Fig. 7 Hole and electron overlap (h/e) in the singlet and triplet excited state of **3BPy-*m*DCz**, **3BPy-*m*DTA**, **3BPy-*m*DMAC** and **3BPy-*m*DPT**, respectively, with the corresponding obtained energy state.

Table 3 Calculation of the rate constants in the 7 wt% emitter:host doped film

Doped film[a]	$k_{P(total)}$[b] (10^7 s^{-1})	k_r[b] (10^7 s^{-1})	k_{IC}[b] (10^7 s^{-1})	k_{ISC}[b] (10^7 s^{-1})	k_{RISC}[b] (10^3 s^{-1})
3BPy-*m*DCz	9.64	5.43	3.71	0.50	3.09
3BPy-*m*DTA	14.61	2.28	2.44	9.88	3.93
3BPy-*m*DMAC	3.23	1.10	0.96	1.16	169.17
3BPy-*m*DPT	6.19	0.44	3.28	2.46	40.04

[a] 7 wt% Emitter: host (DPEPO for **3BPy-*m*DCz** and *m*CBP for the rest three). [b] $k_{P(total)}$, k_r, k_{IC}, k_{ISC}, k_{RISC} are the decay rate constant of total prompt component, radiative decay, non-radiative internal conversion, intersystem crossing and reverse intersystem crossing, respectively.

3BPy-*m*DTA has the optimum value of both the rate constants; hence it shows the highest performance. The experimental result further validates the superiority of **3BPy-*m*DTA** molecular design. Therefore, the computational as well as experimental results strongly indicate that the influence of number and nature of intermediate states between S_1 and T_1 is very crucial to get high EQE.

3. Conclusion

In summary, we have successfully designed and synthesized a series of D–A based molecules (**3BPy-*m*DCz**, **3BPy-*m*DTA**, **3BPy-*m*DMAC** and **3BPy-*m*DPT**) with TADF properties *via* architecture with 3BPy as an unaltered acceptor core and carbazole to phenothiazine as donor moieties. The ΔE_{ST} values came out to be 0.22, 0.20, 0.11 and 0.14 eV for **3BPy-*m*DCz**, **3BPy-*m*DTA**, **3BPy-*m*DMAC** and **3BPy-*m*DPT**, respectively. Consequently, the PLQYs of the doped films were considerably decreased from 59% to 12% upon increasing order of the donor strengths. The doped thin films transient PL decay and electroluminescence results confirm that these compounds are TADF emitters. Upon increasing the donor strength of the TADF emitter, the light emission is tuned from blue (473 nm) to yellow colour (566 nm). Despite relatively large ΔE_{ST} of 0.20 eV in the case of **3BPy-*m*DTA**, the highest performance of the OLED device was achieved on account of maximum exciton utilization leading to an EQE_{max} of 22.5%. This contrast can be attributed to the synergistic effect of both k_{RISC} and k_r by controlling the molecular engineering with an efficient mixing of high-lying ^{3}LE and ^{3}CT. We have demonstrated a systematic molecular design strategy to realize high efficiency *via* controlling the number and nature of intermediate states present between S_1 and T_1, which can act as steps to increase RISC. This work could guide subsequent designing ideas by managing energy level alignments to enable exciton utilization and thus open up a new pathway towards the development of ultra-high efficiency TADF OLEDs.

Conflicts of interest

The authors declare no conflict of interest.

Acknowledgements

The authors are grateful to the Department of Science and Technology (DSTFIST: SR/FST/PSII009/2010) for the instrumental facility at MRC, IISc Bangalore, and SAMat Research Facilities, JNCASR, Bangalore for lifetime measurement facilities on a payment basis. N.Y. and U.D. thank IISc for the doctoral fellowship. Bahadur thanks IISc Bangalore for the C. V. Raman Fellowship. P. R. thanks IISc and the Science & Engineering Research Board (SERB), India, for the SERB-Power Grant (SPG) (Grant No: SPG/2020/000107), Rekha Rao Young Investigator and IGSTC WISER award for financial support.

References

1 H. Uoyama, K. Goushi, K. Shizu, H. Nomura and C. Adachi, *Nature*, 2012, **492**, 234–238.
2 Z. Yang, Z. Mao, Z. Xie, Y. Zhang, S. Liu, J. Zhao, J. Xu, Z. Chi and M. P. Aldred, *Chem. Soc. Rev.*, 2017, **46**, 915–1016.
3 Y. Im, M. Kim, Y. J. Cho, J.-A. Seo, K. S. Yook and J. Y. Lee, *Chem. Mater.*, 2017, **29**, 1946–1963.
4 T. Huang, W. Jiang and L. Duan, *J. Mater. Chem. C*, 2018, **6**, 5577–5596.
5 Y. Liu, C. Li, Z. Ren, S. Yan and M. R. Bryce, *Nat. Rev. Mater.*, 2018, **3**, 18020.
6 S. K. Jeon, H. L. Lee, K. S. Yook and J. Y. Lee, *Adv. Mater.*, 2019, **31**, 1803524.
7 D. Zhong, Y. Yu, D. Song, X. Yang, Y. Zhang, X. Chen, G. Zhou and Z. Wu, *ACS Appl. Mater. Interfaces*, 2019, **11**, 27112–27124.
8 D. Song, Y. Yu, L. Yue, D. Zhong, Y. Zhang, X. Yang, Y. Sun, G. Zhou and Z. Wu, *J. Mater. Chem. C*, 2019, **7**, 11953–11963.
9 S. Hirata, Y. Sakai, K. Masui, H. Tanaka, S. Y. Lee, H. Nomura, N. Nakamura, M. Yasumatsu, H. Nakanotani, Q. Zhang, K. Shizu, H. Miyazaki and C. Adachi, *Nat. Mater.*, 2015, **14**, 330–336.
10 K. Goushi, K. Yoshida, K. Sato and C. Adachi, *Nat. Photonics*, 2012, **6**, 253–258.
11 A. Endo, K. Sato, K. Yoshimura, T. Kai, A. Kawada, H. Miyazaki and C. Adachi, *Appl. Phys. Lett.*, 2011, **98**, 083302.
12 Z. Liu, F. Cao, T. Tsuboi, Y. Yue, C. Deng, X. Ni, W. Sun and Q. Zhang, *J. Mater. Chem. C*, 2018, **6**, 7728–7733.
13 J. Wei, C. Zhang, D. Zhang, Y. Zhang, Z. Liu, Z. Li, G. Yu and L. Duan, *Angew. Chem.*, 2021, **133**, 12377–12381.
14 P. L. dos Santos, J. S. Ward, D. G. Congrave, A. S. Batsanov, J. Eng, J. E. Stacey, T. J. Penfold, A. P. Monkman and M. R. Bryce, *Adv. Sci.*, 2018, **5**, 1700989.
15 X. Tang, L.-S. Cui, H.-C. Li, A. J. Gillett, F. Auras, Y.-K. Qu, C. Zhong, S. T. E. Jones, Z.-Q. Jiang, R. H. Friend and L.-S. Liao, *Nat. Mater.*, 2020, **19**, 1332–1338.

16 B. Milián-Medina and J. Gierschner, *Org. Electron.*, 2012, **13**, 985–991.
17 Y. Olivier, M. Moral, L. Muccioli and J.-C. Sancho-García, *J. Mater. Chem. C*, 2017, **5**, 5718–5729.
18 M. Y. Wong and E. Zysman-Colman, *Adv. Mater.*, 2017, **29**, 1605444.
19 S. Schott, E. R. McNellis, C. B. Nielsen, H.-Y. Chen, S. Watanabe, H. Tanaka, I. McCulloch, K. Takimiya, J. Sinova and H. Sirringhaus, *Nat. Commun.*, 2017, **8**, 15200.
20 J.-A. Lin, S.-W. Li, Z.-Y. Liu, D.-G. Chen, C.-Y. Huang, Y.-C. Wei, Y.-Y. Chen, Z.-H. Tsai, C.-Y. Lo, W.-Y. Hung, K.-T. Wong and P.-T. Chou, *Chem. Mater.*, 2019, **31**, 5981–5992.
21 S. K. Lower and M. A. El-Sayed, *Chem. Rev.*, 1966, **66**, 199–241.
22 Y. Olivier, B. Yurash, L. Muccioli, G. D'Avino, O. Mikhnenko, J. C. Sancho-García, C. Adachi, T.-Q. Nguyen and D. Beljonne, *Phys. Rev. Mater.*, 2017, **1**, 075602.
23 M. K. Etherington, J. Gibson, H. F. Higginbotham, T. J. Penfold and A. P. Monkman, *Nat. Commun.*, 2016, **7**, 13680.
24 P. K. Samanta, D. Kim, V. Coropceanu and J.-L. Brédas, *J. Am. Chem. Soc.*, 2017, **139**, 4042–4051.
25 F. B. Dias, J. Santos, D. R. Graves, P. Data, R. S. Nobuyasu, M. A. Fox, A. S. Batsanov, T. Palmeira, M. N. Berberan-Santos, M. R. Bryce and A. P. Monkman, *Adv. Sci.*, 2016, **3**, 1600080.
26 P. Data, P. Pander, M. Okazaki, Y. Takeda, S. Minakata and A. P. Monkman, *Angew. Chem., Int. Ed.*, 2016, **55**, 5739–5744.
27 T. J. Penfold, E. Gindensperger, C. Daniel and C. M. Marian, *Chem. Rev.*, 2018, **118**, 6975–7025.
28 J. Gibson, A. P. Monkman and T. J. Penfold, *ChemPhysChem*, 2016, **17**, 2956–2961.
29 M. Baba, *J. Phys. Chem. A*, 2011, **115**, 9514–9519.
30 Q. Zhang, J. Li, K. Shizu, S. Huang, S. Hirata, H. Miyazaki and C. Adachi, *J. Am. Chem. Soc.*, 2012, **134**, 14706–14709.
31 K. Shizu, H. Tanaka, M. Uejima, T. Sato, K. Tanaka, H. Kaji and C. Adachi, *J. Phys. Chem. C*, 2015, **119**, 1291–1297.
32 P. Data, P. Pander, M. Lapkowski, A. Swist, J. Soloducho, R. R. Reghu and J. V. Grazulevicius, *Electrochim. Acta*, 2014, **128**, 430–438.
33 *Principles of Fluorescence Spectroscopy*, ed. J. R. Lakowicz, Springer, US, Boston, MA, 2006.
34 P. Rajamalli, N. Senthilkumar, P. Gandeepan, P.-Y. Huang, M.-J. Huang, C.-Z. Ren-Wu, C.-Y. Yang, M.-J. Chiu, L.-K. Chu, H.-W. Lin and C.-H. Cheng, *J. Am. Chem. Soc.*, 2016, **138**, 628–634.
35 J. Zhou, Q. Liu, W. Feng, Y. Sun and F. Li, *Chem. Rev.*, 2015, **115**, 395–465.
36 H. Tanaka, K. Shizu, H. Miyazaki and C. Adachi, *Chem. Commun.*, 2012, **48**, 11392.
37 Q. Zhang, T. Komino, S. Huang, S. Matsunami, K. Goushi and C. Adachi, *Adv. Funct. Mater.*, 2012, **22**, 2327–2336.
38 S.-J. Su, T. Chiba, T. Takeda and J. Kido, *Adv. Mater.*, 2008, **20**, 2125–2130.
39 S. Zhang, L. Yao, Q. Peng, W. Li, Y. Pan, R. Xiao, Y. Gao, C. Gu, Z. Wang, P. Lu, F. Li, S. Su, B. Yang and Y. Ma, *Adv. Funct. Mater.*, 2015, **25**, 1755–1762.
40 F. B. Dias, K. N. Bourdakos, V. Jankus, K. C. Moss, K. T. Kamtekar, V. Bhalla, J. Santos, M. R. Bryce and A. P. Monkman, *Adv. Mater.*, 2013, **25**, 3707–3714.

